



HAL
open science

Dynamic response of epoxy foam structures reinforced with aramid layers subjected to low-velocity impact

Lara Boutros, Pablo Navarro, Steven Marguet, Issam Tawk, Jean-François Ferrero

► **To cite this version:**

Lara Boutros, Pablo Navarro, Steven Marguet, Issam Tawk, Jean-François Ferrero. Dynamic response of epoxy foam structures reinforced with aramid layers subjected to low-velocity impact. Proceedings of the Institution of Mechanical Engineers, Part L: Journal of Materials: Design and Applications, inPress, 10.1177/14644207231199353 . hal-04195193

HAL Id: hal-04195193

<https://hal.science/hal-04195193>

Submitted on 4 Sep 2023

HAL is a multi-disciplinary open access archive for the deposit and dissemination of scientific research documents, whether they are published or not. The documents may come from teaching and research institutions in France or abroad, or from public or private research centers.

L'archive ouverte pluridisciplinaire **HAL**, est destinée au dépôt et à la diffusion de documents scientifiques de niveau recherche, publiés ou non, émanant des établissements d'enseignement et de recherche français ou étrangers, des laboratoires publics ou privés.

Dynamic response of epoxy foam structures reinforced with aramid layers subjected to low velocity impact

L. Boutros^{1,2}, P. Navarro², S. Marguet², I. Tawk¹, J.F. Ferrero²

¹University of Balamand, Lebanon, Al Kourah

² Université de Toulouse, Institut Clément Ader, CNRS/UPS/INSA/ISAE/Mines Albi, 3 rue
Caroline Aigle, 31400 Toulouse, France

Abstract:

This study investigates the impact response of epoxy foam structures reinforced with aramid woven fabrics through drop weight tests. These structures are not classical sandwich panels as the fabrics are blended into the epoxy foam. The number of aramid plies and their location are varied, and the influence of the foam density is studied. Low-velocity drop weight tests are conducted. The load-displacement curves, the morphology of damage, the indentation and the back face signature (BFS) are analyzed. Results reveal that increasing the number of aramid layers in the middle of the structure reduces the crack propagation and increases the peak load. In addition, adding one layer of aramid at the back face prevents the crack propagation. Finally, the use of several foam densities, with the higher density at the impact face leads to an improved protection capacity.

Keywords:

Hybrid structures

Low-velocity impact

Woven composite

Epoxy foam

1. Introduction

Cellular materials are lightweight materials used in several engineering areas: thermal insulation, electromagnetic interference shielding for electric components, and core material for sandwich-type composite materials. As these materials have low mechanical properties in terms of stiffness and strength, they are usually combined with structural materials, for example carbon/epoxy composites, in order to build hybrid or sandwich structures with high mechanical capabilities. When submitted to crash or impact loading, the cellular part of these structures generally undergoes very large deformations.

Foam materials are built from various base materials like polymers, metals, ceramics or glasses [1]. The fabrication process of polymer foams is generally done in two steps: mixing and molding [2]. The foaming process can be achieved through mechanical, physical, or chemical foaming [3]. Mechanical foaming consists in mixing the liquid polymer until emulsified. Then for physical foaming, a low boiling point agent should be added to the polymer before mixing to create the foam

system. Finally, the chemical foaming is when two chemical solutions are added together and mixed mechanically. At this point, a chemical reaction occurs and produces gases. Afterward, the polymer is foamed by pressuring and heating. Polymer foams can be categorized according to their raw material: thermoplastic, thermoset, and elastomers. Thermoplastic foams can include, Polystyrene, Polyethylene, and Polyvinyl chloride; thermoset foams include, Polyurethane, Phenolic resin, and Epoxy resin [2]. One advantage of using epoxy-based foam is that it can be combined easily during the manufacturing process with epoxy based composite laminates.

The mechanical behavior of polymer foams strongly depends on the manufacturing process, base material, morphology of the microstructure, and density [1]. Under compressive loading, all-polymer foam stress-strain curves show three different regions: linear-elastic region, plateau region, and densification region [4, 5]. The linear elastic region is governed by the bending of the cell walls, where the Young's modulus of the foam manages the slope of this linear behavior. The collapse of the cells characterizes the plateau region; elastic buckling for elastomeric foams and brittle crushing for brittle foams such as ceramic or epoxides. When all the cells are crushed or compacted, an increase in stress describes the densification region. The foam response to tensile stress is first linear elastic controlled by bending and stretching the cell walls. Elastomeric foams show a linear behavior. Plastic foams attain a yield point and presents non-linear behavior until failure. Brittle foams show a significant brittle failure after the elastic region with cracks propagating rapidly throughout the structure. As for the cell microstructures, two types exist: closed cell and open cell [6]. A closed-cell foam consists of a wall surrounding all the cells, separating them from one another. Open-cell walls are open to each other, making it impossible to entrap gas or liquid inside. As a result of the cell microstructure, closed cells tend to be stiffer, the cell geometry resists air leakage and shows more strength than open cells, that tends to be softer [7, 8]. The tensile response of polymer foams is also connected to the foam density. It is usually observed that it governs the mechanical properties of polymer foam: as the density of the foam increases, the mechanical properties increase [6, 9].

Foam behavior under dynamic loading is sensitive to the strain rate. Yan et al. studied the influence of the strain rate on the behavior of polymer foams under compressive loading [10]. It was shown that when the strain rate increases, the plateau stress increases, and the densification appears sooner. One explanation is that the behavior of the polymer foams is monitored by the speed at which the air escapes the foam cells [1].

This sensitivity to the loading rate coupled with the ability of the foam to handle very large strain in compression provides advanced energy-absorption capacity toward impact loading [11,12]. The

behavior of polymer foams under impact can be analyzed through the impact load versus impactor displacement curve and a visual inspection of the sample. Impact starts with a localized deformation underneath the indenter, followed by a buckling and collapse of the cells. Then, the damage propagates with mainly buckling and collapses but also with the apparition of cracks, mainly in shearing. Energy absorption occurs by cell fracture and crushing [4, 13]. Nevertheless, due to the relatively low mechanical properties of the foams, the amount of energy that can be absorbed by this material remains generally much lower than the impact energy.

The improvement of the mechanical properties of the foams in order to increase the potential in future applications has been the subject of recent studies. Reinforcement of polymer foams can be achieved by integrating fillers and reinforcing particles during manufacturing [14]. Fillers are solid particles that are typically used in small quantities to enhance the value of the foam. Three main particles type are generally used: fibrous fillers (glass fiber, aramid fiber, and carbon fiber), nanofillers (nanoclays, graphite nanotubes), and rubber particles. Reinforcements aim to obtain mechanical properties superior to those obtained in ordinary foams. Improvements include an increase in modulus, strength, and energy absorption; modulation of electrical properties; and tailoring thermal properties such as thermal expansion, thermal conductivity, and glass transition temperature (T_g) [15].

Fibrous fillers can be in the form of chopped strands of fiber filament. Which act to reinforce the foam by switching the stress from the low stiffness foam to the fibers [16]. Yang et al. [17] studied the behavior of Polypropylene (PP) thermoplastic foam reinforced by short glass fibers (diameter of about 13 μm). The study proves that adding around a 20% wt ratio of glass fibers to the PP foam improves the tensile strength, the tensile modulus, the specific bending stress, and modulus by 59.45%, 54.81%, 94.75%, and 82.42%, respectively, compared to neat PP foam. As for short carbon fibers, Wenzhe et al. [18] show that adding short carbon fibers to epoxy foam improves the fracture toughness up to 113% compared to neat epoxy foam. Organic fiber can also be a successful additive to polymer foams; studies dealing with Kenaf fiber [19] and bamboo fiber [20] as a reinforcement show that their addition improves the mechanical and thermal properties of the foam compared to the ordinary foam.

Carbon Nanotubes, Nanofibers, and rubber particles as reinforcement are also very popular since they have low density due to their hollow core [14]. Awad et al. [21] and Kumar et al. [22] both study the addition of carbon nanotubes to polymers foams. Both studies prove that adding nanoparticles improves the mechanical properties (tensile strength and modulus) and thermal stability.

Nevertheless, adding reinforcement into the epoxy foams might increase the fracture toughness. The introduction of fillers lead to a significant decrease in the compressive strength compared to neat unreinforced foam [18]. In addition, adding silica particles to polyurethane foam in a high concentration shows a decrease in tensile strength compared to neat foam [23]. Javni et al. [24] show that the reinforcement of polyurethane foam with Nano-silica improves the hardness and compression strength but decreases the rebound resilience. On the other hand, adding filler during the preparation of polymer foam faces several challenges on the fabrication level, especially in maintaining a uniform dispersion inside the foam media and the orientation of the nanoparticles [13].

In the present study, the enhancement of the impact behavior is investigated at the structural level, without modifying the microstructure of the foam. The reinforcement is realized by adding aramid woven composite fabric within epoxy foam layers. Thus, the need of sophisticated mixing techniques is avoided and the manufacture process is highly simplified. The fabric is selected based on its high impact strength and its high impact energy absorption capability. The number of aramid layers across the thickness and their position along the thickness direction are varied in order to study their ability to change the impact behavior and morphology of damage towards low velocity impact loading. Foam layers of different density were also used between the plies. The capacity of energy absorption and the ability of protection is assessed. It is shown that adding one aramid ply at bottom layer highly reduces the size of the cracks in the foam material, that structures with a higher number of aramid plies in the middle attain higher peak load and that impact face foam density influences the stiffness and impact performance of the structure.

2. Experimental procedure




The tested configurations include structures made of foams without reinforcement called “neat foams”, structures having one or three aramid plies in the middle or distributed in different locations in the thickness of the specimen, and finally, structures having two foam densities separated in the middle by one or three aramid plies. The impact behavior of the structures is analysed based on impact load versus impactor displacement curves, on the damage morphology, on the indentation depth and on the level of protection. The level of protection corresponds to the structure's ability to reduce local loading of the protected part which is directly behind it. It is assessed classically by placing a clay witness material underneath the structure during impact [25]. After impact, the indentation depth measured on the clay, also called Back Face Signature (BFS), indicates the level of protection that the structures can achieve. The clay witness material used is a Plastiline provided by Herbin with a hardness index of 50.

2.1 Manufacturing of the structures and presentation of the impacted configurations

Three different densities of epoxy foam are studied: 170, 250, and 400 kg/m³. The epoxy foam used is provided by Sicomin [26]. The epoxy foams used are bi-component (PB/DM03) closed-cell foams with different expansion rates. As the components are mixed, they expand due to chemical foaming. The aramid fibers are a four harness satin woven fabric with an areal density of 175 g/m² and a thickness of 0.26 mm, supplied by Hexcel with the reference HexForce 20914. The matrix is an Araldite LY 5052 (resin)/Aradur 5052 (hardener) epoxy from Huntsman. The weight ratio fibers over resin is 50:50. The aramid plies are impregnated with a wet layup process. Then the epoxy foam mix is prepared. The structures are fabricated inside a closed mold. The impregnated aramid plies are fixed on the edges of the mold to be stabilized during the expansion of the foam and the polymerization. The foam was not pre-formed in order to obtain a better bonding with the aramid plies due to a partial penetration of the epoxy foam inside the plies during process. Afterwards, the mold is placed in a hot air oven at 40°C for 12 hours. Finally, the samples are cut using a water jet-cutting machine into square structures of 100mm×100mm. The thickness is 30 mm.






In order to study of the influence of the number of aramid plies on the impact response, nine configurations were fabricated. The structures are manufactured with the same foam through the thickness, with no aramid ply (“PB-neat”), one aramid ply (“PB-1ply-PB”) or three aramid plies (“PB-3plies-PB”) in the middle (Table 1). Each configuration is fabricated with the three different foam densities (170, 250, and 400 kg/m³).

Table 1: Mono-foam density structure with aramid plies in the middle and neat foam

configuration	[PB-1ply-PB]	[PB-3plies-PB]	[PB-neat]
representation			

















Then, in order to study of the influence of the position of the aramid plies on the impact behavior, fifteen configurations were manufactured (Table 2). Two configurations are reinforced with only one layer of aramid: on the top (“1ply-PB”) or on the bottom (“PB-1ply”). Three other configurations are built with three layers of aramid: one ply on the top and two in the middle (“1ply-PB-2plies-PB”), two in the middle and one on the bottom (“PB-2plies-PB-1ply”), and finally one on the top, one in the middle and one on the bottom (“1ply-PB-1ply-PB-1ply”).

Table 2: Mono-foam density structure with aramid plies distributed in different locations

configuration	[1ply-PB]	[PB-1ply]	[1ply-PB-2plies-PB]	[PB-2plies-PB-1ply]	[1ply-PB-1ply-PB-1ply]
representation					

Finally, the influence of the foam density on the impact response is studied with structures having one or three plies in the middle but with two foams with different densities (bi-foam) (Table 3). In this case, the upper foam part of the structure has a different density than the bottom part. Each pair of foams corresponds to two configurations: one configuration where the impacted face is the foam with the lowest density and a second configuration where the impacted face is the foam with the highest density. Twelve combinations are fabricated, combining PB250 and PB170, PB400 and PB170, and finally, PB400 and PB250.

Table 3: Bi-foam density structure with aramid plies in the middle

[PB170-1ply-PB250]	[PB170-1ply-PB400]	[PB250-1ply-PB400]
		
[PB250-1ply-PB170]	[PB400-1ply-PB170]	[PB400-1ply-PB250]
		
[PB170-3plies-PB250]	[PB170-3plies-PB400]	[PB250-3plies-PB400]
		
[PB250-3plies-PB170]	[PB400-3plies-PB170]	[PB400-3plies-PB250]
		
Legend		
 PB170	 PB250	 PB400
 Aramid ply		

2.2 Drop weight impact test

The study of the impact damage mechanisms is investigated through low-velocity impact tests. The experimental conditions are defined on the basis of the ASTM D7136 standard concerning impact resistance of composite laminates [27]. A hemispherical-end steelhead with a mass of 2 kg and a diameter of 16 mm impacts the structures. The velocity of the impact is 6 m/s, equivalent to an impact energy of 36 J. The structures are simply placed on a soft clay material in order to be able to measure the indentation left on the clay after the impact, also known as Back Face Signature (BFS). The 25mm thick clay material is stabilized inside a home-made wooden box. In order to be consistent with the classic tests using BFS measures, the clay is heated before the test to reach a

temperature of around 38°C. A schematic design of the test setup and mounting are shown in Figure 1. Potential rebound that could lead to multiple impact is prevented. The impact load and the impactor displacement are recorded during the test. The outputs of the drop weight test are the following: visual inspection of the structures, load-displacement curves, permanent indentation, and BFS. Two tests were performed for each configuration to check repeatability. The difference between the impact results of the two tests were lower than 4% for each configuration. As it is presented in part 3, this variation is small compared to the variations measured between two configurations.

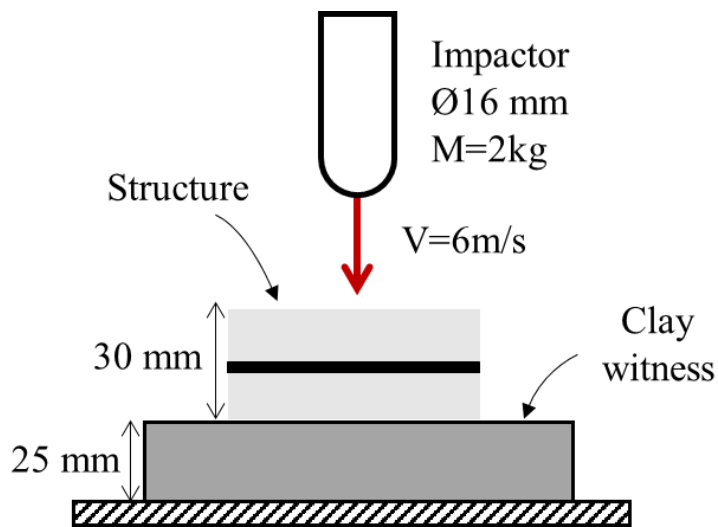


Figure 1: Experimental setup of drop weight impact test

3. Results and discussion

3.1 Impact response of neat epoxy foams

The load-displacement curves are given in Figure 2. The linear phase of the load-displacement curve indicates the elastic response of the epoxy foam. The slight change of slope observed afterward describes the bending and crushing of the foam cells, where most of the impact energy is dissipated. Finally, a significant drop of load occurs when the epoxy foam fails. Foam density plays an essential role in the impact response. As the density increases, the peak load and the stiffness in the linear phase also increase.

All three structures with different densities show the same morphology of damage. Figure 2.b shows the post-impact state of the [PB250-neat] specimen. The impact leads to brittle failure, which tears the epoxy foam into pieces. The severity of the crack is due to the high cross-linked density in all epoxides materials [28].

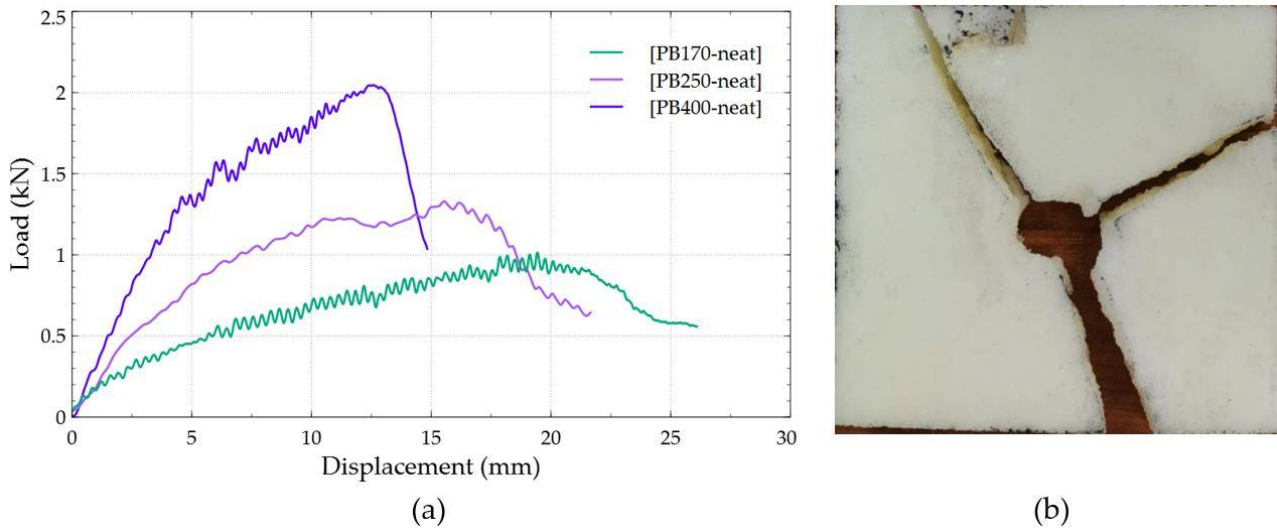


Figure 2: a) Load-displacement curves of neat epoxy foam, b) Bottom view of [PB250-neat]

3.2 Influence of the number of aramid plies

This section demonstrates the effect of the number of aramid layers in the middle of mono-foam structures. The load-displacement curves of the PB170, PB250, and PB400 with one and three aramid plies in the middle are plotted in Figure 3.

For PB170 structures (Figure 3.a), the behavior is the same for the three configurations until a displacement of 10mm. Then the slope increases for the specimens that contains aramid layers. Indeed, for these two configurations, foam densification occurs between the impactor and the first layer of aramid. The load reaches a maximum of 2.1kN for the configuration with 3 plies and 1.95kN for sample with 1 ply. It corresponds to an increase of respectively 110% and 95% compared to the neat foam sample [PB170-neat]. Then a load drop occurs, which means that the aramid plies fail. A second drop in load indicates the failure of the epoxy foam on the bottom of the specimen. The decrease of the displacement at the end of the graph corresponds to the beginning of the rebound of the impactor. Adding one or three aramid plies in the middle delays the complete rupture of the structures and increases the peak load.

The same influence is observed on the response of the samples made of PB250 foam (Figure 3.b). Nevertheless, for the structure with three aramid plies, no drop in load is observed. Indeed, for this configuration the aramid layers were not fully broken.

Finally, for the two configurations made with PB400 foam and aramid plies, the slope of the load-displacement curve is higher than for the [PB400-neat] sample from the beginning of the loading (Figure 3.c). Indeed, in that case, the stiffness of the foam itself is high enough to load the aramid plies before the crushing of the foam. Moreover, for these two samples, the impactor rebounds before the complete failure of the aramid layers.

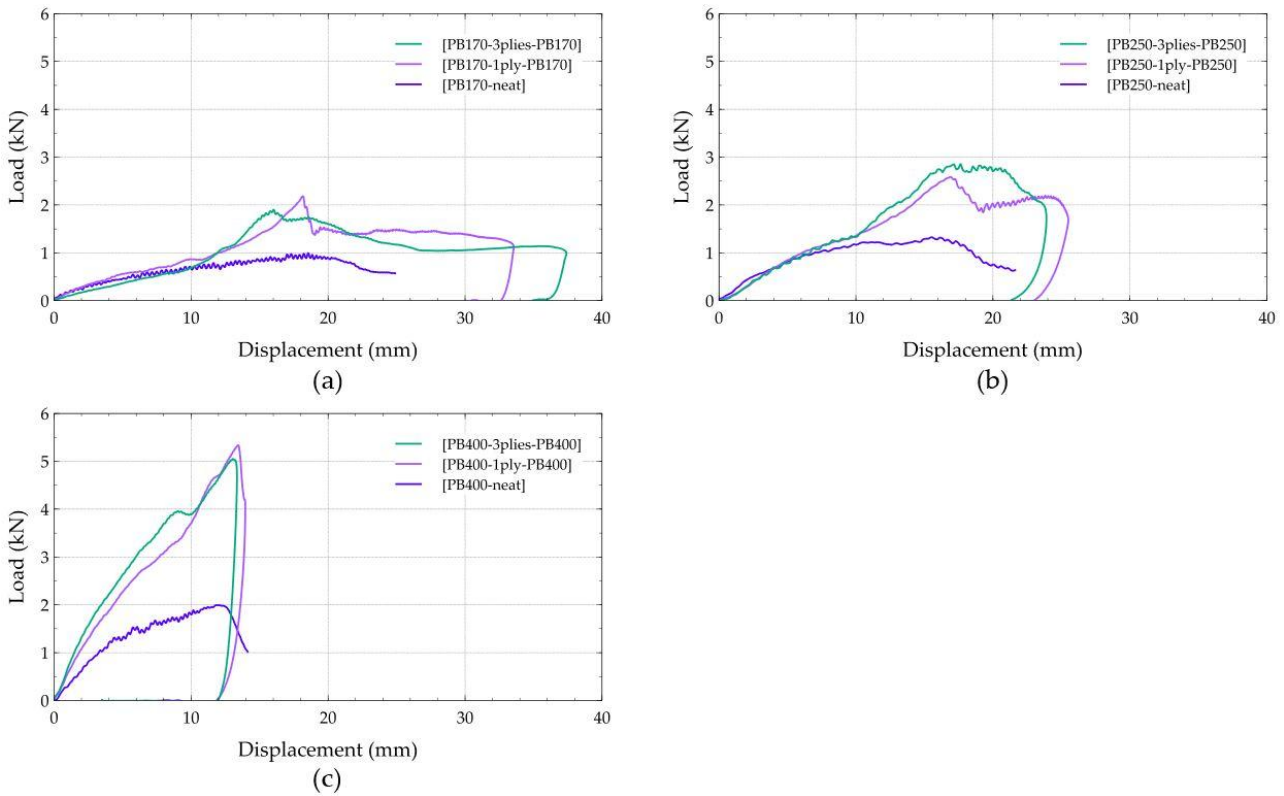


Figure 3: Load-displacement curves for mono foam structures with aramid plies in the middle: a) PB170 foam, b) PB250 foam, c) PB400 foam

Figure 4 compares the morphology of the damage of the six mono-foam configurations with one or three aramid layers at the middle. It is shown that all structures with PB170 are fully perforated. A clear hole is formed on the impact and bottom face with a diameter of around 16 mm. Then, for structures having PB250, a clear hole is observed on the upper layer. Fiber breakage and matrix cracking are noticed in the structure having 1 ply of aramid in the middle, leading to a perforation of the aramid. The deformation of the aramid fiber in a conical shape. The foam of the lower face presents a brittle failure with large cracks and a debonding between the aramid and the foam. For the PB250 structure with three aramid plies in the middle, a plug of densified foam is noticed under the impactor mark. Aramid plies are not perforated, but crack propagation and debonding are also noticed. Finally, concerning the PB400 samples, only the one having one aramid ply in the middle presents cracks on the bottom face, whereas the one having three aramid plies only shows the damage caused by the indenter on the impact face. The PB400 governs the behavior of these structures since the indenter rebounds before perforating the aramid layers.

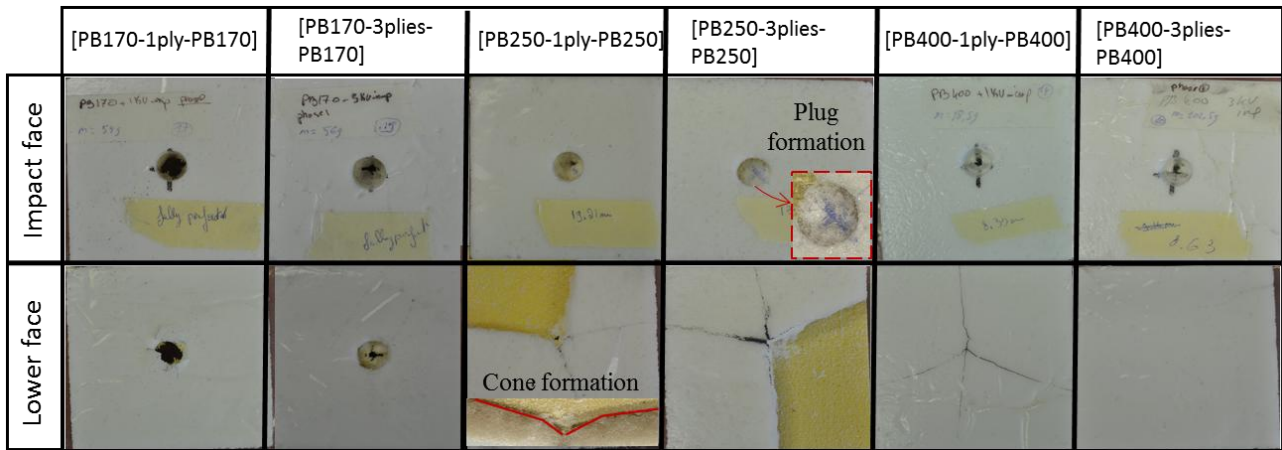


Figure 4: Morphology of the damage to structures having one or three aramid plies in the middle

The BFS depth measurement, that quantifies the ability of the structure to provide protection, is given Figure 5. As the structures with PB170 are fully perforated, the BFS cannot give any significance and is not plotted. Concerning structures with PB250, the three aramid plies have a BFS 21% lower compared to the structure with only one aramid ply. As for PB400, since the indenter is stopped at the first layer of epoxy foam, there is no significant deformation on the back face.

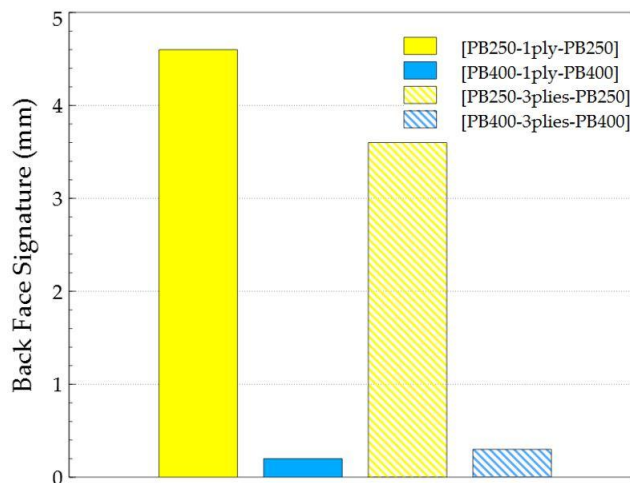


Figure 5: Back face signature of mono-foam structures with aramid plies in the middle

The presence of aramid layers in the middle of the structure have an important influence on the impact behavior of the epoxy foams. Indeed, it tends to increase the impact peak load and to lower the amount of cracks in the foam. Moreover, for the sample with PB250 foam and three plies in the middle and the two samples with PB400 foam and aramid layers, the addition of aramid woven plies make it possible to stop the impactor.

3.3 Influence of aramid plies location

This section deals about the effect of the position of the aramid layers on the impact response of the epoxy foam/aramid structures. The configuration used to carry out this study are those presented in Table 2. The analyze will be done first with PB170 specimen, then with PB250 specimen and finally with PB400 specimen.

Figure 6 presents the load-displacement curves for the PB170 epoxy foam samples with one or three plies with different distribution through the thickness. For the samples with one aramid layer located on top, middle or bottom, an influence on the position and on the value of the peak load is observed. Indeed, the peak load corresponds to the failure of the aramid ply. Thus, it is observed in the load-displacement curve of Figure 6.a with a peak load at 2mm for [1ply-PB170], at 16.5mm for [PB170-1ply-PB170] and 32mm for [PB170-1ply]. When the aramid ply is on top, the load reached at the aramid failure is 65% lower than the load reached in the two other configurations. More, for these two configurations, an increase of the slope just before the peak load is observed. It is due to local densification of the foam. Concerning the value of the displacement needed to stop the impactor, the best configuration is [PB170-1ply-PB170] with a maximum displacement of 33mm. The sample with a ply at the bottom stops the impactor with a displacement 3% higher while the sample with a ply on top fails to stop the impactor.

Figure 6.b also analyses the influence of modifying the location of the three-aramid plies. Equally, to the analysis above, the failure of the plies is well identified in the load-displacement curves with the sudden drops of load. The maximum peak load value is measured for sample [PB170-3plies-PB170] where three aramid plies are stacked together at the middle. Contrary to the other three configurations, sample [1ply-PB170-2plies-PB170] does not manage to stop the projectile. If we compare with [PB170-2plies-PB170-1ply] configuration, which is the same ply repartition but not impacted on the same face, it can be noticed again that putting a ply on top is not really relevant.

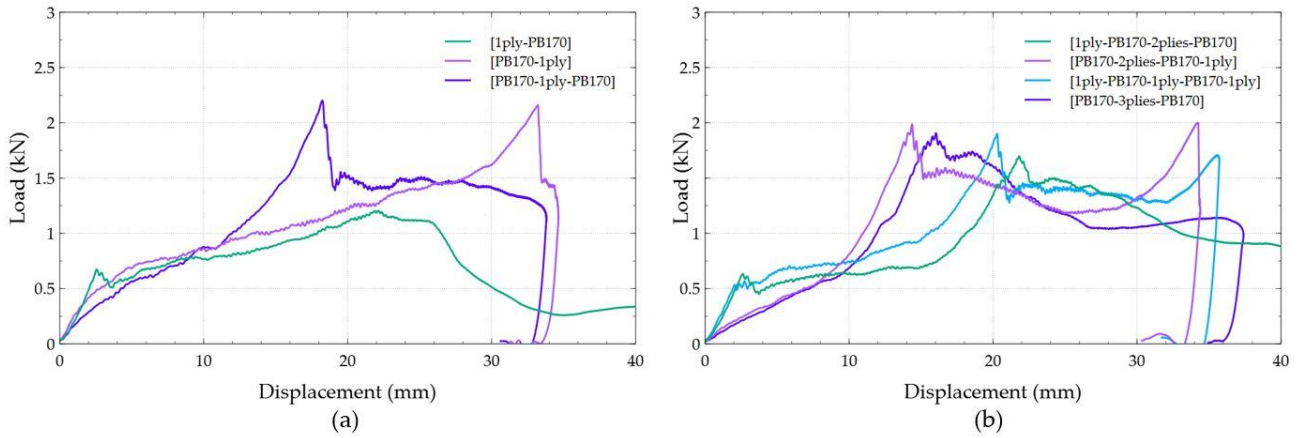


Figure 6: Load-displacement curves for mono foam PB170 structures with a) 1ply either on top, at the middle or at the bottom and b) 3plies distributed differently in the structure

The morphology of the damage for five specimens is presented in Figure 7. Structure [1ply-PB170] shows clear propagation of the cracks on the lower face. For the structure with one aramid ply on the bottom, no crack propagation is noticed in the foam. However, a cross shape failure of the aramid ply is observed. Yet, [1ply-PB170-2plies-PB170] is fully perforated similarly to [PB170-3plies-PB170]. [PB170-2plies-PB170-1ply] and [1ply-PB170-1ply-PB170-1ply] only show a slight deformation on the bottom face. Thus, the presence of a ply on the bottom face improves the impact response, contributing to hindering the crack propagation on the bottom face of the structures.

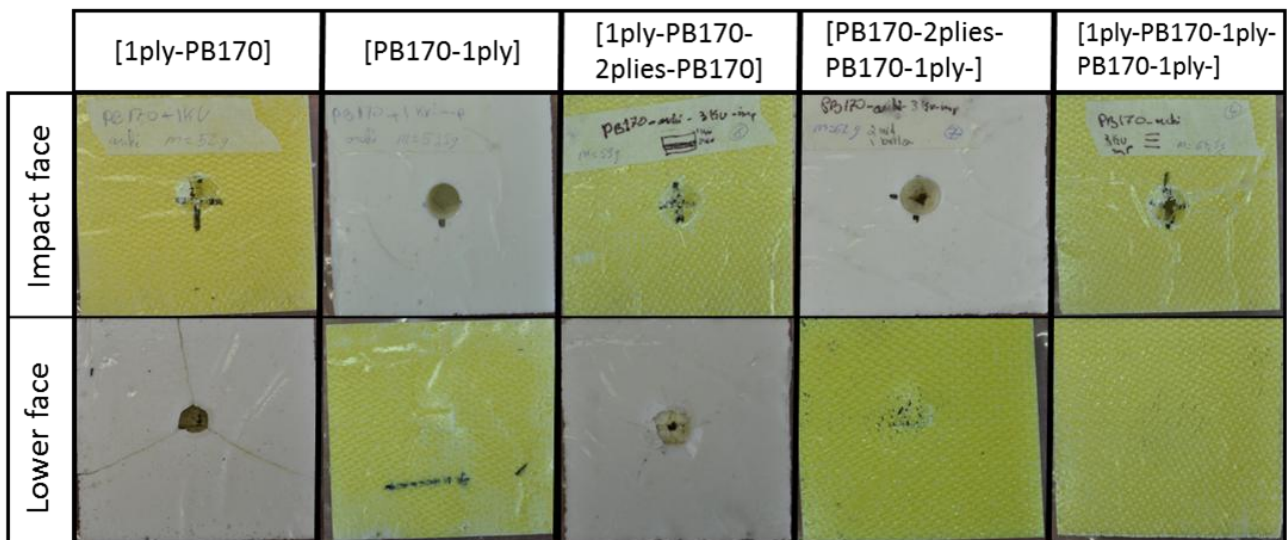


Figure 7: Morphology of the damage for mono-foam PB170 structure with aramid plies in different locations

The amount of deformation that the structures left on the soft clay are illustrated in Figure 8. As the configurations [PB170-1ply-PB170], [PB170-3plies-PB170] and [1ply-PB170-2plies-PB170] are fully perforated, the values of the BFS are not reported. The structure protected by an aramid ply at the bottom shows the lower BFS. In particular, structures with three aramid plies distributed in the

top, middle, and bottom present the lowest BFS. The addition of aramid ply on the bottom does not only avoids the cracks in the foam but also decreases the BFS.

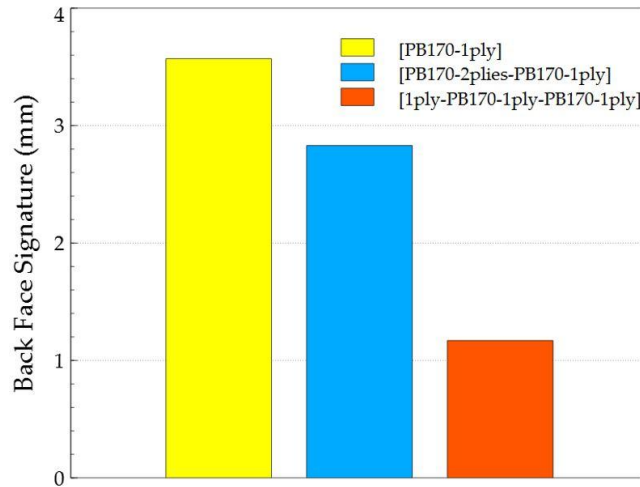


Figure 8: Back face signature of mono-foam PB170 structures with aramid plies in different locations

Figure 9 shows the load-displacement curves of structures with PB250 reinforced with one or three aramid plies in different locations. The same main behavior described before with the PB170 structures is observed. Figure 9.a shows that the structure with a ply on top is unable to stop the projectile, while [PB250-1ply-PB250] and [PB250-1ply] shows a maximal displacement of 22.5mm and 24mm respectively. Then, it can be observed on Figure 9.b that the structures with three plies could stop the impactor at a displacement of around 20 mm. The structure having aramid ply on top possess higher initial stiffness. Structure [PB250-3plies-PB250] show similar behavior as [PB250-2plies-PB250-1ply]. This means that increasing the number of aramid plies in the middle does not change the global response.

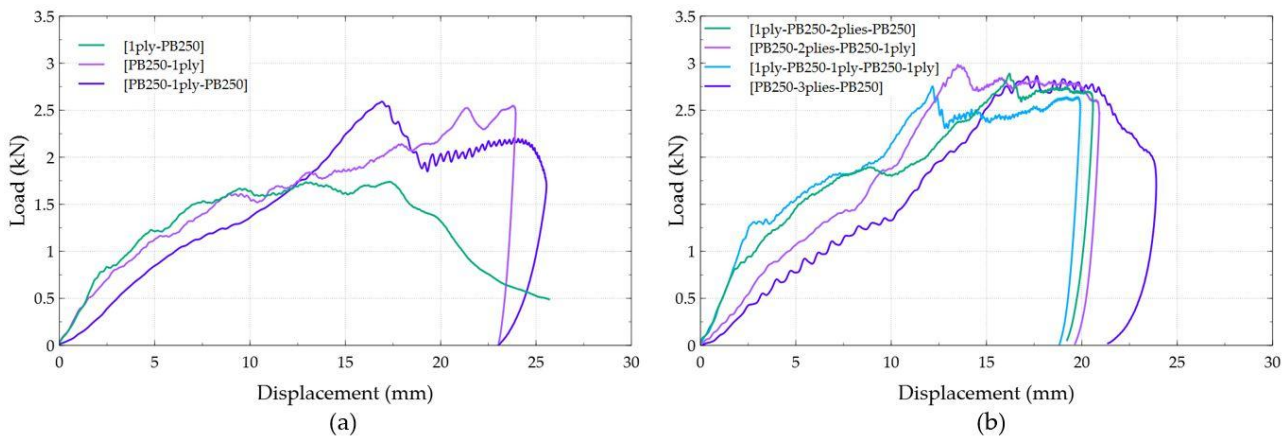


Figure 9: Load-displacement curves for mono foam PB250 structures with aramid plies in different locations

The morphology of damage to those structures is similar with the one found in Figure 7, which reveals that when adding aramid ply on the bottom, the epoxy foam is reinforced and does not

display cracks or brittle failure. Nevertheless, non-zero BFS is measured. Indeed, the BFS is mainly due to the local bending of the structure. Even if the epoxy foam does not present large cracks, it is locally damaged and crushed so that the structure locally deforms during impact. Figure 10 presents the BFS of the PB250 structures. The structure having one aramid ply on the impact face fails similarly to [PB250-neat]. As it is fully perforated, the values of the BFS are not reported. The structure having one aramid ply on the bottom significantly improves BFS. Nevertheless, [1ply-PB250-2plies-PB250] does not possess a ply at the bottom, it still has better BFS than [PB250-1ply] by 31%. This is due to the aramid plies on top and in the middle, which increase the stiffness and peak load of the structure. [PB250-2plies-PB250-1ply] and [1ply-PB250-1ply-PB250-1ply] only show a slight BFS located on the four edges of the structure due to its sinking inside the clay. Therefore, it does not imply damage in the location of the load applied.

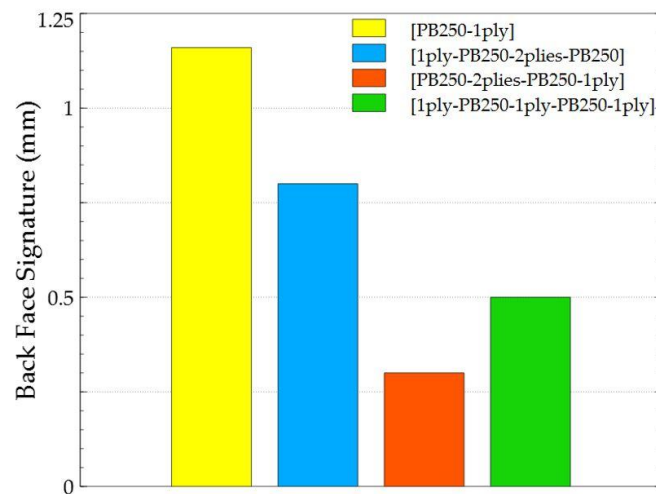


Figure 10: Back face signature of mono-foam PB250 structures with aramid plies in different locations

For a structure with PB400, the influence of aramid location is not illustrated clearly, as shown in Figure 11. Indeed, as the density and the mechanical characteristics of PB400 are higher, the aramid plies located at the middle or at the bottom of the structure do not influence the global response. The impactor is stopped, leaving no back face signature other than the edges of the structure. Only structure [1ply-PB400] results in complete perforation towards the impact.

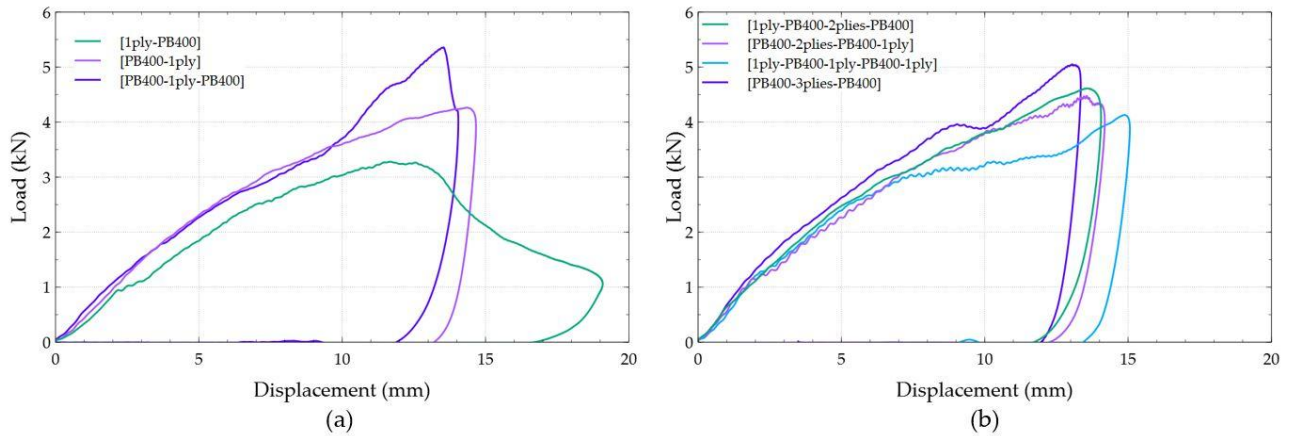


Figure 11: Load-displacement curves for mono foam PB400 structures with aramid plies in different

These results underline the importance of the location of aramid plies inside the structure. An improvement in crack propagation was observed when a ply of aramid was added on the bottom face of the structure, where it reinforces the epoxy foam by hindering crack propagation. Additionally, it was established that adding one ply of aramid on top could increase the initial stiffness of the structure. Those improvements also manifest in the BFS, which decreases when the brittle failure of the epoxy foam is avoided. However, the foam density also plays a significant role in improving the back face signature. The structure having PB170 with aramid one ply on the bottom shows a higher back face signature by 68% compared to the same configuration structure with PB250. More, Figure 12 shows the permanent indentation of the configuration [1ply-PB-1ply-PB-1ply] with the three different averaged densities. These results confirm that the BFS is improved when the density of foam increases and the permanent indentation left inside the structure after the impact is significantly improved by up to 47%. However, the total density of the structure is increased by 70%. In order to account for the mass of the structure when analyzing the impact performance, the ratio *margin/mass* (mm/g) has been introduced. The margin is defined by the plate thickness at the impacted location minus the indentation depth left by the indenter inside the structures. It corresponds to the minimal distance between the target and the impactor during the impact. This ratio aims to compare the structures with different global densities. It helps to study the ability of the structures to stop the indenter while taking into account their mass. The higher the ratio is, the more effective the structure is against the impact. Figure 12.c shows that the configuration with the PB400 foam has a margin/mass ratio respectively 6% and 89% higher than the configurations with PB170 and PB250 foam.

The influence of density variation inside a single structure is studied in the next section to investigate the potential of decreasing the density of a structure while keeping the same performance towards impact.

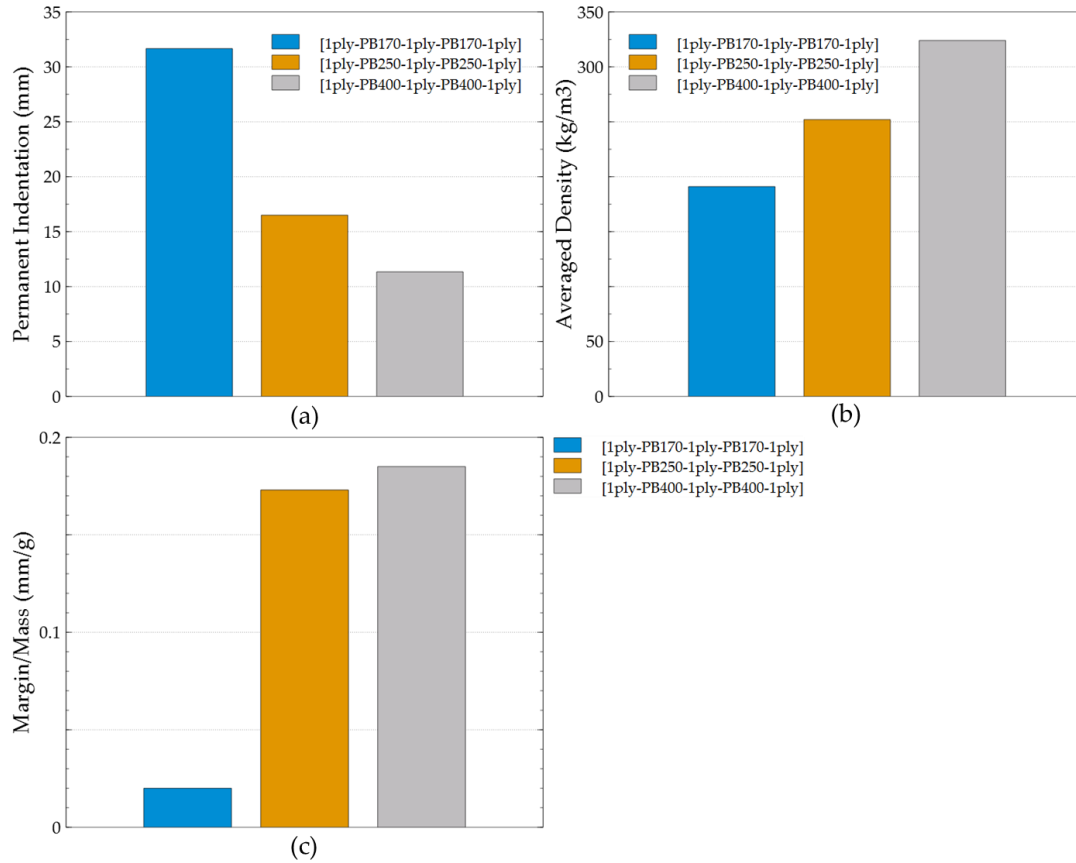


Figure 12: a) Permanent indentation, b) density and c) Mass/Margin ratio of configuration [1ply-PB-1ply-PB-1ply]

3.4 Influence of foam density variation

The following section compares mono-foam and bi-foam structures with three aramid plies in the middle. This comparison aims to evaluate the influence of the variation of the epoxy foam density inside a single structure. In this section, three combinations are studied, PB170/PB250, PB170/PB400, and PB250/PB400.

In addition to the load-displacement curves, permanent indentation values and BFS, the influence of the epoxy foam density is also studied by calculating the ratio *margin/mass* (mm/g). Figure 13 compares the behavior of bi-foam structures PB170 and PB250 in a single structure. It presents load-displacement curves, permanent indentation, averaged densities ρ , margin/mass ratio and BFS for four configurations. The first one, where PB170 is on top and PB250 is on the bottom, is called [PB170-3plies-PB250]. The second configuration is the reverse [PB250-3plies-PB170]. The two last configurations are mono-foam samples, presented for comparison purposes. The load-displacement curves show that the structure having PB250 on top has improved initial stiffness, peak load and maximal displacement by 120%, 17% and 20% respectively, compared to the other bi-foam structure. The permanent indentation and BFS of [PB250-3plies-PB170] compared to [PB170-3plies-PB250] is decreased by 30% and 74% respectively while the margin/mass ratio is

40% higher. The load-displacement curves shows that the behavior for [PB250-3plies-PB170] and [PB250-3plies-PB250] is very similar, however this later shows a higher BFS of 200%. This is due to crack propagations in the PB250 foam located on the bottom, leaving a higher BFS as pieces of foam penetrating the clay. On the contrary, [PB250-3plies-PB170] has higher permanent indentation than [PB250-3plies-PB250]. This is explained by the local crushing of the PB170 foam under the impactor.

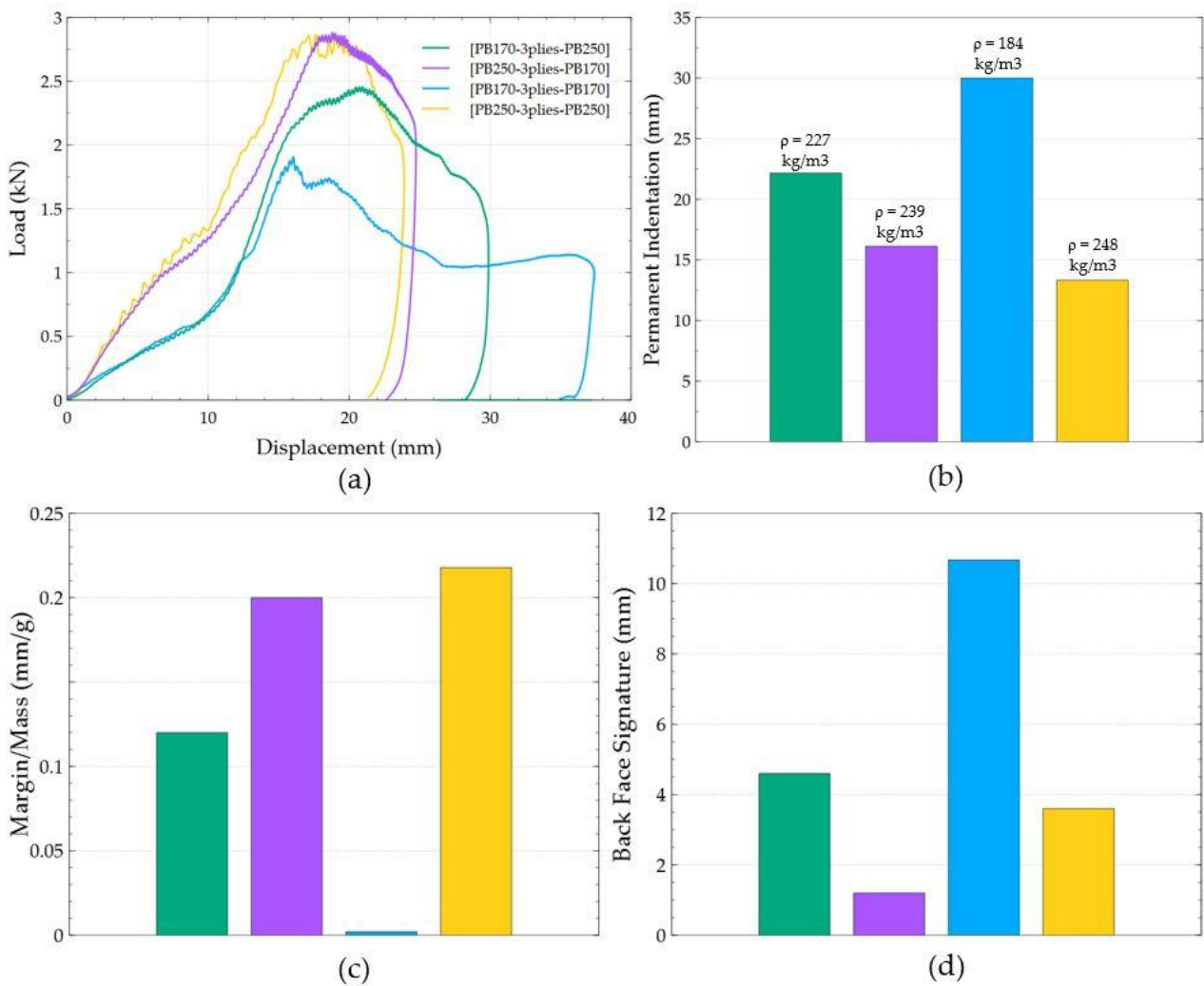


Figure 13: (a) Load-displacement curves, (b) Permanent indentations and averaged densities, (c) mass/margin ratios and (d) BFS of PB170/PB250 with three aramid plies.

Figure 14 deals with the response of PB170 and PB400 structures. The perforation of [PB170-3plies-PB170] can be prevented by replacing the bottom foam by PB400. However, replacing the upper foam with PB400 instead of PB170 prevents perforation and increases the stiffness by 480%. The structure configuration [PB400-3plies-PB170] also improves permanent indentation,

margin/mass ratio and BFS compared to [PB170-3plies-PB400] by about 48%, 29% and 87%, respectively. On the other hand, comparing the mono-foam structure, [PB400-3plies-PB400], with [PB400-3plies-PB170], both have very similar behavior and the indentation; however, the structure having PB170 as the bottom layer shows a reduced relative density by around 9%.

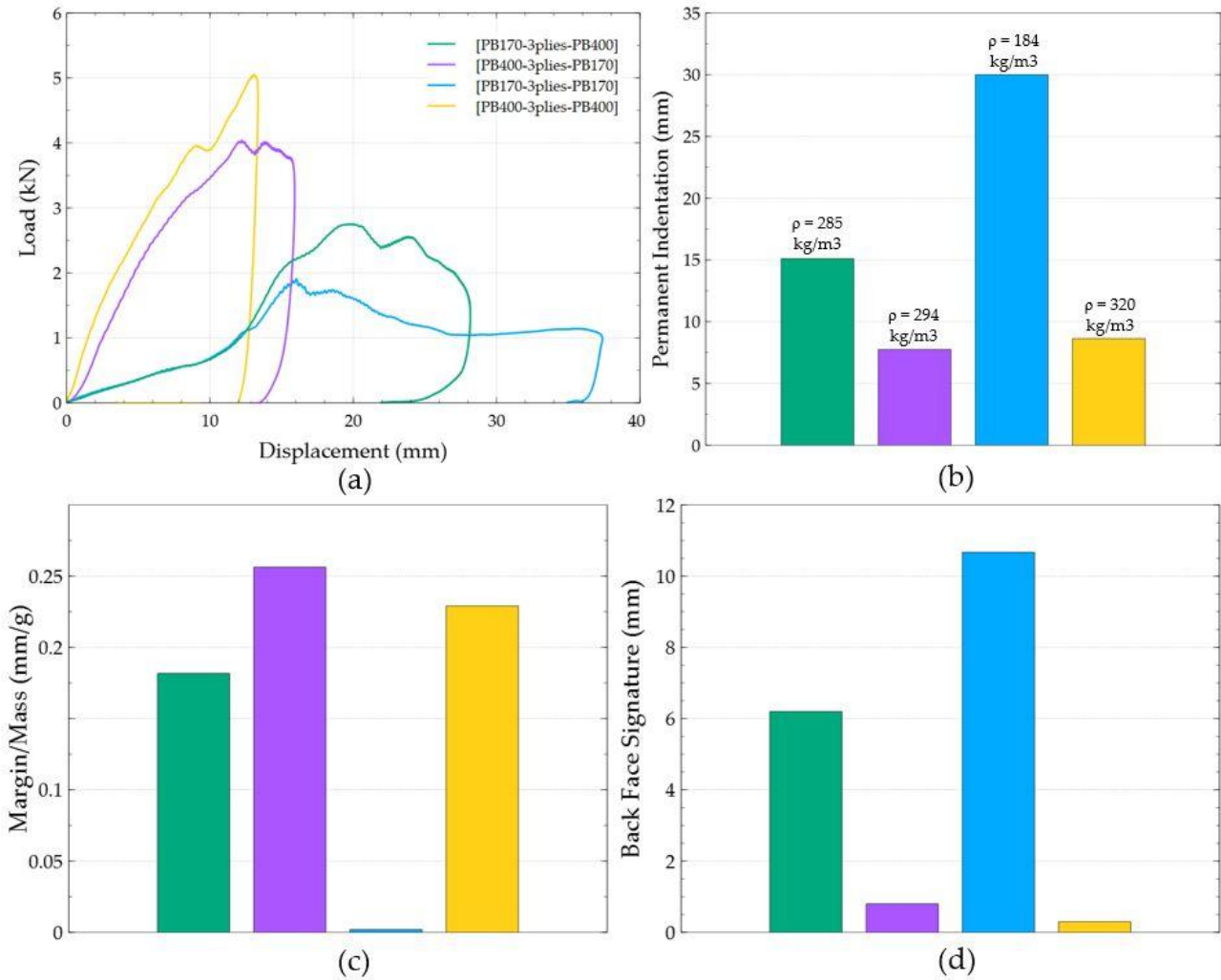


Figure 14: (a) Load-displacement curves, (b) Permanent indentations and averaged densities, (c) mass/margin ratios and (d) BFS of PB170/PB400 with three Aramid plies.

Figure 15 presents structures with PB400 and PB250 with three aramid plies in the middle. It can be shown on the load-displacement curve that the structure [PB250-3plies-PB250] has a similar behavior as [PB250-3plies-PB400]. Comparing it with [PB400-3plies-PB250], an increase of the initial stiffness occurs by 178%. In the case of the structures having PB400 as the top layer, the aramid plies in the middle do not play a significant role since the impactor does not even reach them.

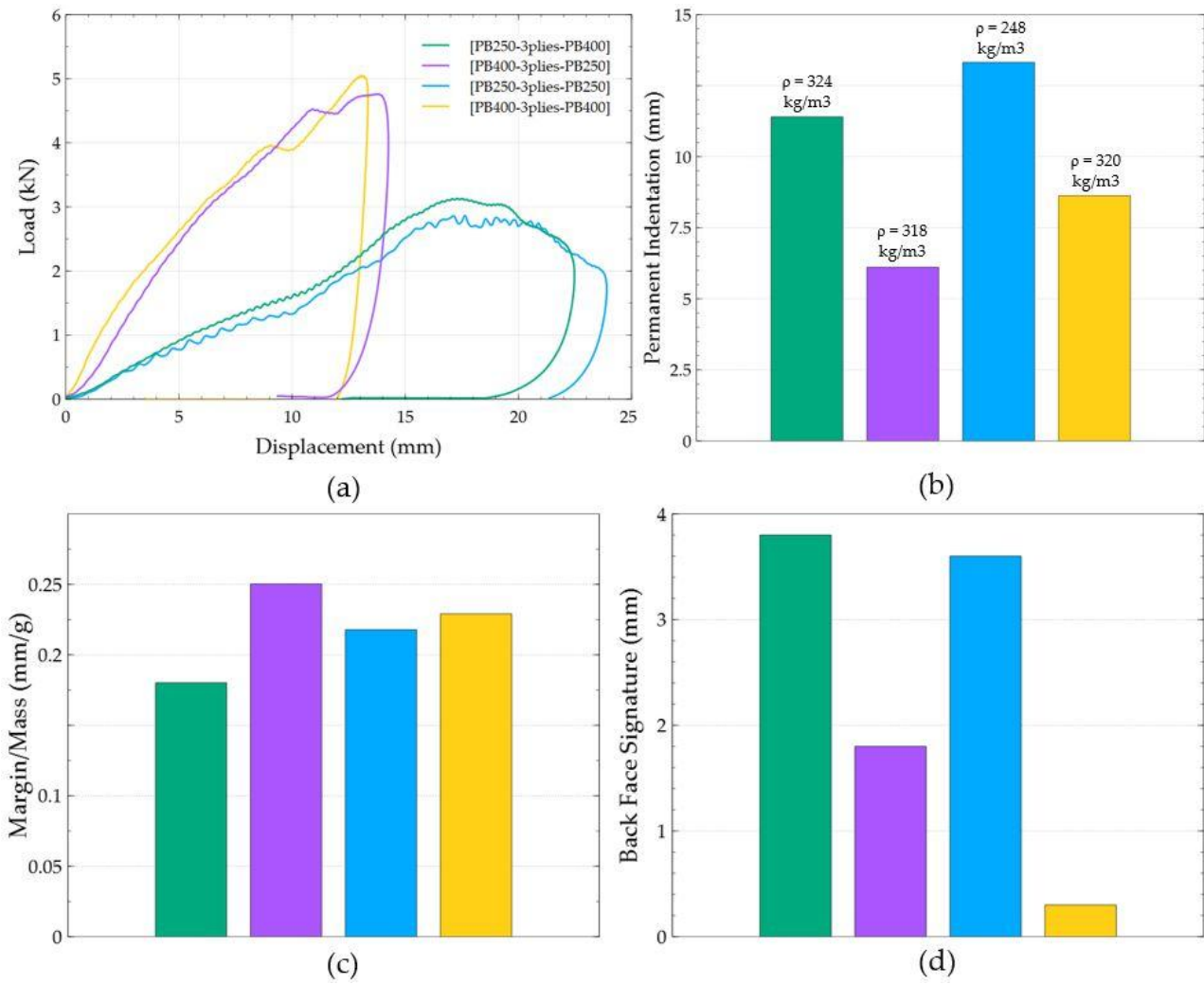


Figure 15: (a) Load-displacement curves, (b) Permanent indentations and averaged densities, (c) mass/margin ratios and (d) BFS of PB250/PB400 with three Aramid plies.

Finally, in order to have a global comparison of performances, the results of the margin/mass ratio for the configurations with the foam with the higher density on top are presented in Figure 16.

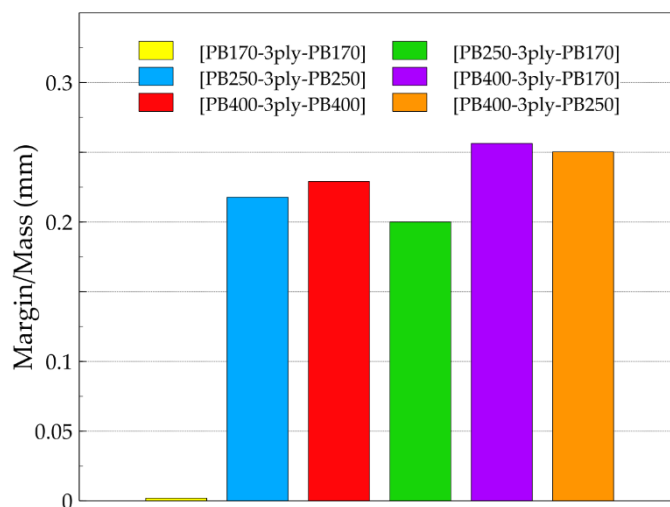


Figure 16: Margin over mass ratio for mono and bi-foam structures

[PB170-3plies-PB170] has the lowest weight and exhibits the lowest ratio, since the structure is fully perforated. Replacing the impact face by PB250 obviously increases the ratio. However, structure [PB250-3plies-PB250] has an increased ratio by 9% compared to [PB250-3plies-PB170]. This is due to the presence of PB170 on the back face, which leads to higher permanent indentation.

For structures with PB400 as impact face, whether mono or bi-foams structures, the ratio is higher than the rest of the structures. However, structures with PB400 as the impact face with PB170 or PB250 as the back face show an increased ratio of 12% and 8%, respectively, compared to [PB400-3plies-PB400]. This means that bi-foam structures with PB400 show a better capacity to stop the indenter per unit mass than mono-foam structures with PB400. The structure that maximizes this ratio the most is [PB400-3plies-PB170].

The findings presented in this section show that a structure having a higher foam density as an impact face shows higher initial stiffness and yields better permanent indentation and BFS while having the same global density of the structure. Having the lowest foam density as impact face leads to full penetration of the upper foam, damage of the aramid plies, and a cone formation on the bottom face, ending with cracks propagation on the bottom face of the PB400. Figure 17 illustrates the damage morphology inside both structures combining PB170 and PB400. The failure of the aramid plies in the middle is represented by a cone formation on the lower face, leading to a brittle failure of the bottom layer of epoxy foam.

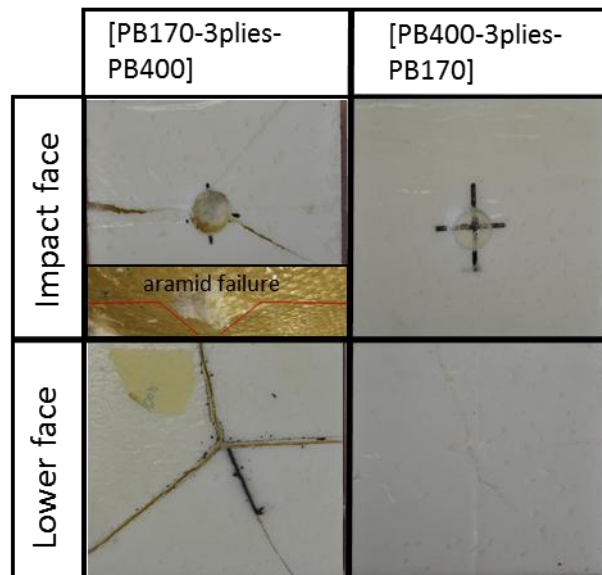


Figure 17: Morphology of the damage to bi-foam PB170/PB400 structure with three aramid plies in the middle

However, even when adding a higher foam as the top face, which monitors mainly the behavior of the structure, it could not obstruct the crack propagation due to the brittleness of the structures.

3.5 Summary

The main results deduced from the analysis of the low-velocity impact tests performed on the studied hybrid epoxy-foam/aramid fabrics structures are listed here:

- As the foam density increases, its capacity to carry load increases as well.
- One or three aramid plies in the middle of the epoxy foam improve the behavior by decreasing the crack propagation and by increasing the peak load.
- Aramid plies location can significantly influence the morphology of damage inside the structure by controlling its stiffness when added to the top face or by protecting the bottom face from crack propagation.
- Structures with two different foams and with 3 plies of aramid in the middle are monitored by the behavior of the top layer foam density. Having the highest density as top face proved enough to stop the indenter with minimum damage left of the clay (BFS) compared to the structures having low-density foam as the top face.
- The analysis of the ratio between the margin and the mass shows that replacing the impact face density of mono-foam structures with a higher density improves the ability to stop the indenter per unit mass. However, in the case of PB400 as an impact face, replacing the bottom foam layer with lower foam density improves the protection level per unit mass.

4. Conclusion

The behavior of epoxy foam reinforced by aramid layers was investigated experimentally through low-velocity impact tests. Several configurations were tested to study the influence of the location and number of aramid plies and the foam density variation inside a single structure. The comparison and analysis are based on load-displacement curves, damage morphology, permanent indentation and BFS. The main outcomes are the following:

1. Foam density indicates the capacity of load carrying, where PB400 shows higher mechanical properties since it has a higher density. However, for all the foams studied, neat epoxy foam fails with significant brittleness due to crack propagation.
2. Adding one or three aramid plies to the PB170 does not prevent complete perforation but induces a different damage mode. However, for PB250 and PB400 adding the plies in the middle prevent perforation. Increasing the aramid plies in the middle shows higher peak load and less crack propagation on the bottom.
3. Crack propagation is only prevented for all foam densities when one ply of aramid is added to the bottom face of the structure. This ply plays a significant role by hindering crack propagation.

4. The damage propagation scenario inside the structures starts when the indenter crushes the upper part of the foam. When the impactor reaches the aramid plies, it causes a failure represented by matrix cracks, fiber breakage, and cone formation on the lower face of the aramid plies. This damage induces the failure of the lower part of the structure.
5. Foam density influences and monitors the behavior of the structures, especially when the highest density is located at the impact face. Structures with the configuration [PB250-3plies-PB170], [PB400-3plies-PB250], and [PB400-3plies-PB170] show better impact behavior. Substituting the bottom layer of the mono-foam PB400 with PB250 or PB170 can guarantee the same stiffness and approximately comparable indentation levels while saving weight.
6. A ratio *margin/mass* is introduced in order to measure the specific ability of the structure to stop the indenter. Structures with PB400 as impact face exhibit the highest ratio, meaning the best protection level per unit mass. Replacing the bottom layer of [PB400-3plies-PB400] with PB170 or PB250 keeps the same level of protection while decreasing the mass by 24%.

This study demonstrates that the strategy that consists in reinforcing a light material like a foam with fabrics is promising for protection applications. Indeed, modifying the number and location of aramid plies while varying the epoxy foam density can significantly improve the impact response of the structures.

References

1. Gibson LJ. Cellular solids. *Mrs Bulletin* 2003; 28: 270-274.
2. Liu PS, and Chen GF. *Porous materials: processing and applications*. Elsevier. 2014.
3. Jin FL, Zhao M, Park M, et al. Recent trends of foaming in polymer processing: A review. *Polymers* 2019; 11: 953.
4. Gibson LJ and Ashby MF. *Cellular solids structure & properties*. 2nd ed. Cambridge University Press. 1997.
5. Eaves D. *Handbook of polymer foams*. Rapra Technology Ltd. 2004.
6. Drobny JG. *Handbook of thermoplastic elastomers*. Elsevier. 2014.
7. Kaewunruen S, Ngamkhanong C, Papaelias M, et al. Wet/dry influence on behaviors of closed-cell polymeric cross-linked foams under static, dynamic and impact loads. *Construction and Building Materials* 2018; 187: 1092-1102.
8. Mills N. *Polymer foams handbook: engineering and biomechanics applications and design guide*. Elsevier. 2007.
9. Feng D and Aymerich F. Effect of core density on the low-velocity impact response of foam-based sandwich composites. *Composite Structures* 2020; 239: 112040.
10. Yang LM and Shim VPW. A visco-hyperelastic constitutive description of elastomeric foam. *International journal of impact engineering* 2004; 30: 1099-1110.
11. Viana JC. Polymeric materials for impact and energy dissipation. *Plastics Rubber and Composites* 2006; 35: 260-267.
12. Tomin M and Kmetty Á. Polymer foams as advanced energy absorbing materials for sports applications - a review. *J. Applied Polymer Science* 2022; 139: 51714.
13. Michler GH and Balta-Calleja FJ. *Mechanical properties of polymers based on nanostructure and morphology*. Taylor and Francis. 2016.
14. Dong Y, Umer R and Lau AKT. *Fillers and reinforcements for advanced nanocomposites*. Woodhead Publishing. 2015.
15. Gupta N, Pinisetty D and Shunmugasamy VC. *Reinforced polymer matrix syntactic foams: effect of nano and micro-scale reinforcement*. Springer. 2013.
16. Murphy J. *Additives for plastics handbook*. Elsevier. 2001.
17. Yang C, Wang G, Zhao J et al. Lightweight and strong glass fiber reinforced polypropylene composite foams achieved by mold-opening microcellular injection molding. *Journal of Materials Research and Technology* 2021; 14: 2920-2931.
18. Song W, Konstantellos G, Li D et al. Short carbon fibre-reinforced epoxy foams with isotropic cellular structure and anisotropic mechanical response produced from liquid foam templates. *Composites Science and Technology* 2019; 184: 107871.
19. Hassan NAA, Ahmad S, Chen RS et al. Synergistically Enhanced Mechanical, Combustion and Acoustic Properties of Biopolymer Composite Foams Reinforcement by Kenaf Fibre. *Composites Part A: Applied Science and Manufacturing* 2022; 155: 106826.
20. Tang Q, Fang L and Guo W. Effects of bamboo fiber length and loading on mechanical, thermal and pulverization properties of phenolic foam composites. *J. Bioresources and Bioproducts* 2019; 4: 51-59.

21. Awad SA, Fellows CM and Mahini SS. Effects of accelerated weathering on the chemical, mechanical, thermal and morphological properties of an epoxy/multi-walled carbon nanotube composite. *Polymer Testing* 2018; 66: 70-77.
22. Kumar SV, Subramanian J, Giridharan A et al. Processing and characterization of organic PU foam reinforced with nano particles. *Materials Today: Proceedings* 2021; 46: 1077-1084.
23. Nunes RCR, Fonseca JLC and Pereira MR. Polymer–filler interactions and mechanical properties of a polyurethane elastomer. *Polymer testing* 2000; 19: 93-103.
24. Javni I, Zhang W, Karajkov V et al. Effect of nano-and micro-silica fillers on polyurethane foam properties. *Journal of cellular plastics* 2002; 38: 229-239.
25. NIJ Standard–0101.04. Ballistic Resistance of Personal Body Armor.
26. Sicomin. Systèmes époxydes pour production de mousses alvéolaires. <http://sicomin.com/produits/systemes-epoxy/moussage-structurel> (2014, accessed 12 December 2022).
27. ASTM D7136 / D7136M-15. Standard Test Method for Measuring the Damage Resistance of a Fiber-Reinforced Polymer Matrix Composite to a Drop-Weight Impact Event.
28. Bagheri R, Marouf BT and Pearson RA. Rubber-toughened epoxies: a critical review. *Journal of Macromolecular Science, Part C: Polymer Reviews* 2009; 49: 201-225.